Journal of Engineering Mathematics 19 (1985) 139–155.

On the effects of non-linearity in free-surface flow about a submerged point vortex

L.K. FORBES

Department of Mathematics, Kansas State University, Manhattan, KS 66506 USA *

(Received December 6, 1984)

Summary

Two-dimensional free-surface flow about a point vortex in a stream of infinite depth is investigated. The non-linear problem is formulated in terms of an integrodifferential equation on the exact, unknown location of the free surface, and this equation is then solved numerically. The non-linear results are compared with the predictions of linearized theory and, for positive circulation, it is found that the latter may under-estimate the drag force significantly. For negative circulation, the linearized theory grossly over-predicts the value of the wave resistance, which apparently even becomes zero in a limiting configuration.

1. Introduction

This paper is concerned with the effects of non-linearity upon two-dimensional flow about a point vortex immersed beneath the surface of a running stream of infinite depth. The fluid is assumed to be ideal, so that a potential flow problem with non-linear boundary conditions upon a free surface is required to be solved.

Flows due to the motion of mathematical point singularities in a fluid possibly represent the simplest of all problems in hydrodynamics in which a free surface is involved, and consequently, their study has had a long history. Traditionally, these problems have been linearized under the assumption that the strength of the disturbing singularity is small, and the solution obtained by integral-transform techniques. The solutions for point sources, vortices and dipoles in fluids of finite and infinite depth are reviewed by Wehausen and Laitone [1], and the case of fluid of infinite depth is considered in detail by Kochin, Kibel' and Roze [2].

The development of the digital computer has enabled modern-day researchers to embark upon purely numerical solutions to many non-linear free-surface problems, and a recent review article by Yeung [3] is devoted to this subject. Solutions to the non-linear equations describing flow about submerged point singularities have also been undertaken recently. Hess [4] sought to solve the same problem as is considered here, and achieved limited success by making use of a surface-singularity technique. However, the convergence of his iterative scheme for solving the non-linear integral equation of the motion is in some doubt; this would appear to be due to the eigenvalues of the integral equation

* Present address: Department of Mathematics, University of Queensland, St. Lucia, Queensland 4067, Australia.

forming a continuous (uncountable) distribution along the entire negative real axis in the complex eigenvalue plane. This is discussed in greater detail by Forbes [5]. Salvesen and von Kerczek [6] solved the non-linear equations for flow about a point vortex in a stream of finite depth using a finite-difference method, and their results, which are in substantial agreement with our own, will be cited frequently in this paper. Since their method involves the distribution of numerical mesh points throughout the entire fluid, it cannot be used in the present context of infinite fluid depth, unless at least some intermediate change of variables is employed.

In the present paper, a boundary-integral formulation in the plane of the physical variables is employed, and is similar to the approach adopted by Miksis, Vanden Broeck and Keller [7] in that an arclength parametrization of the free surface is utilized. Details of this formulation are provided in Section 2. Note that the inverse formulation of Forbes and Schwartz [8], for example, cannot be used here because of the presence of a stagnation point at an unknown position within the fluid, at which the inverse transformation would become singular. The method employed in this study is therefore available in a much wider class of problems than that used by Forbes and Schwartz, yet with no loss of numerical efficiency. In Section 3 we review the linearized theory, and Section 4 contains the algorithm used for the numerical solution of the non-linear problem. Results are presented in Section 5 and compared with the predictions of linearized theory, and a discussion in Section 6 concludes the paper.

2. Formulation of the problem

We consider a two-dimensional stream of infinite depth flowing from left to right with uniform speed c far upstream, and subject to the downward acceleration g of gravity. A cartesian coordinate system is defined such that the y-axis points vertically, and the x-axis, located at the level of the free surface far upstream, points in the overall direction of the flow. A vortex of strength K is located a distance H beneath the origin, and the free surface generally possesses a uniform train of Stokes waves, radiating downstream to infinity.

The problem is non-dimensionalized using H and c as reference length and speed, respectively. The function $\eta(x)$, which describes the elevation of the free surface, is therefore made dimensionless by reference to H, and the velocity potential ϕ and streamfunction ψ are referred to the product cH. A definition sketch of the non-dimensional flow is given in Figure 1. The two independent dimensionless parameters of the flow are the Froude number $F = c(gH)^{-1/2}$ and vortex strength $\epsilon = K(cH)^{-1}$.

The fluid is assumed to be incompressible and inviscid, and to flow without rotation. Consequently, the velocity potential and streamfunction satisfy the Cauchy-Riemann equations

$$\phi_x = \psi_y, \quad \phi_y = -\psi_x \tag{2.1}$$

everywhere in the fluid except at the vortex itself. Equations (2.1) imply that the complex potential $f = \phi + \mathrm{i}\psi$ should be an analytic function of $z = x + \mathrm{i}y$, except at the vortex, where

$$f \to z + \frac{\mathrm{i}\epsilon}{2\pi} \ln(z + \mathrm{i}) \qquad \text{as} \quad z \to -\mathrm{i}. \tag{2.2}$$

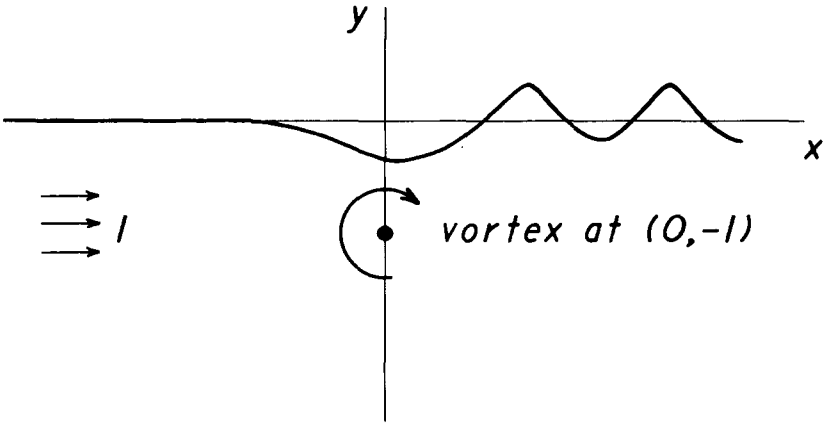

Figure 1. The non-dimensionalized problem and coordinate system.

Far upstream, the fluid obeys the radiation condition

$$f \to z \qquad \text{as} \quad \mathrm{Re}\{z\} \to -\infty, \tag{2.3}$$

and at the free surface $y = \eta(x)$, it is necessary to impose the kinematic boundary condition

$$\phi_x \frac{\mathrm{d}\eta}{\mathrm{d}x} = \phi_y \qquad \text{on} \quad y = \eta(x) \tag{2.4}$$

and the Bernoulli equation

$$\tfrac{1}{2}F^2\left(\phi_x^2 + \phi_y^2\right) + y = \tfrac{1}{2}F^2 \qquad \text{on} \quad y = \eta(x). \tag{2.5}$$

The above problem is reformulated in terms of an integrodifferential equation along the unknown free-surface location, using Cauchy's Integral Formula and the residue theorem. Consider the function

$$\chi(z) = \frac{\mathrm{d}f}{\mathrm{d}z} - 1 \tag{2.6}$$

which vanishes infinitely far upstream, by equation (2.3), and also at infinite depth within the fluid, and which remains bounded far downstream. This function is analytic everywhere in the fluid except at the vortex, $z = -\mathrm{i}$, where it has a simple pole, and consequently,

$$\oint_\Gamma \frac{\chi(\xi)\mathrm{d}\xi}{\xi - z} = 2\pi\mathrm{i}\,\mathrm{Res}\{-\mathrm{i}\}. \tag{2.7}$$

The positively-oriented contour Γ in equation (2.7) is sketched in Figure 2. It consists of the entire free surface except the point z which is by-passed with a semi-circle of vanishingly small radius, and a semi-circle at infinity.

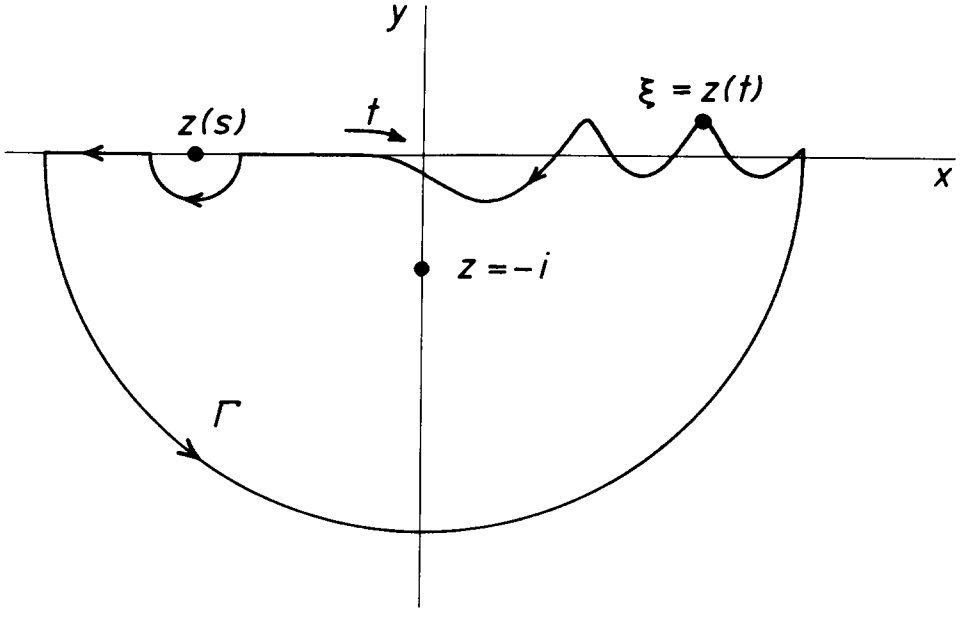

Figure 2. The contour Γ in the complex z-plane.

Let the free surface be parametrized by the arclength t, and suppose that the point z on the surface is obtained when $t = s$. Now the contribution to the integral in equation (2.7) from the semi-circle at infinity is clearly zero, since $\chi(\xi)$ defined in equation (2.6) vanishes along this contour. The contribution from the semi-circle of vanishingly-small radius which is centred at the point z in Figure 2 and traversed clockwise is $-i\pi\chi(z)$; consequently, equation (2.7) becomes

$$i\pi\chi(z(s)) = -\int_{-\infty}^{\infty} \frac{\chi(z(t))z'(t)dt}{z(t)-z(s)} - 2\pi i \,\mathrm{Res}\{-i\}, \tag{2.8}$$

in which the improper integral is to be interpreted in the Cauchy Principal-Value sense.

It remains to evaluate the residue term in equation (2.8). Since the pole of the function $(\xi - z)^{-1}\chi(\xi)$ at $\xi = -i$ is simple, we have

$$\mathrm{Res}\{-i\} = \lim_{\xi \to -i} \frac{(\xi + i)\chi(\xi)}{\xi - z}$$

which, in view of equations (2.2) and (2.6), becomes

$$\mathrm{Res}\{-i\} = -\frac{i\epsilon}{2\pi(z+i)}. \tag{2.9}$$

Consequently, equation (2.8) yields

$$\chi(z(s)) = -\frac{\epsilon}{i\pi(z(s)+i)} - \frac{1}{i\pi}\int_{-\infty}^{\infty} \frac{\chi(z(t))z'(t)dt}{z(t)-z(s)}. \tag{2.10}$$

The desired integrodifferential equation is obtained by taking the real part of equation (2.10). Firstly, however, we note that in terms of arclength s, the kinematic surface condition (2.4) becomes

$$\psi_s = 0 \tag{2.11}$$

and Bernoulli's equation (2.5) gives

$$\tfrac{1}{2}F^2\phi_s^2 + y = \tfrac{1}{2}F^2. \tag{2.12}$$

In addition, the definition of arclength requires that

$$x_s^2 + y_s^2 = 1. \tag{2.13}$$

In view of equations (2.11) and (2.13), the real part of equation (2.10) gives rise to the singular integrodifferential equation

$$\begin{aligned}\phi'(s)x'(s) - 1 &= \frac{\epsilon(y(s)+1)}{\pi\left[x^2(s)+(y(s)+1)^2\right]} \\ &+ \frac{1}{\pi}\int_{-\infty}^{\infty} \frac{[\phi'(t)-x'(t)][y(t)-y(s)]+y'(t)[x(t)-x(s)]}{[x(t)-x(s)]^2+[y(t)-y(s)]^2}\,\mathrm{d}t.\end{aligned} \tag{2.14}$$

The unknown functions $x(s)$, $y(s)$ and $\phi(s)$ at the free surface are therefore obtained by solving the coupled non-linear equations (2.12)–(2.14), subject to the radiation condition (2.3).

Once the above unknown functions have been obtained, the wave-drag D and lift L experienced by the point vortex may be computed from Blasius's first formula (see Batchelor [9], page 433)

$$D - \mathrm{i}L = \tfrac{1}{2}\mathrm{i}F^2 \oint_C \left(\frac{\mathrm{d}f}{\mathrm{d}z}\right)^2 \mathrm{d}z. \tag{2.15}$$

Here, C denotes any positively-oriented simple closed contour lying wholly within the fluid and having the point vortex in its interior, and D and L have been made dimensionless with respect to $\rho g H^2$, where ρ is the fluid density.

Suppose that z_0 is an interior point in the fluid, lying on contour C. Cauchy's integral formula and residue theorem now give

$$\chi(z_0) + \mathrm{Res}\{-\mathrm{i}\} = \frac{1}{2\pi\mathrm{i}} \oint_{\Gamma_0} \frac{\chi(\xi)\mathrm{d}\xi}{\xi - z_0} \tag{2.16}$$

where contour Γ_0 is the same as the contour Γ in Figure 2, except that the small semi-circle bypassing surface point z is now unnecessary. The contribution from the semi-circle at infinity is again zero, and the residue is given by equation (2.9), so that

equation (2.16) becomes

$$\chi(z_0) = -\frac{\epsilon}{2\pi i(z_0+i)} - \frac{1}{2\pi i}\int_{-\infty}^{\infty} \frac{\chi(z(t))z'(t)dt}{z(t)-z_0}.$$

This formula at once yields the derivative df/dz required in equation (2.15), and we write

$$\frac{df}{dz} = -\frac{\epsilon}{2\pi i(z+i)} + \mathcal{G}(z) \tag{2.17a}$$

for all internal points $z = z_0$, where the function

$$\mathcal{G}(z) = 1 - \frac{1}{2\pi i}\int_{-\infty}^{\infty} \frac{\chi(z(t))z'(t)dt}{z(t)-z} \tag{2.17b}$$

is analytic everywhere in the fluid. Substituting equations (2.17) into (2.15) and evaluating the integral by the calculus of residues yields

$$D - iL = -i\epsilon F^2 \mathcal{G}(-i). \tag{2.18}$$

The real and imaginary parts of equation (2.18) finally give the formulae

$$D = \frac{\epsilon F^2}{2\pi}\int_{-\infty}^{\infty} \frac{[\phi'(t)-x'(t)]x(t) - y'(t)[y(t)+1]}{x^2(t)+[y(t)+1]^2}dt \tag{2.19}$$

and

$$L = \epsilon F^2 + \frac{\epsilon F^2}{2\pi}\int_{-\infty}^{\infty} \frac{[\phi'(t)-x'(t)][y(t)+1] + y'(t)x(t)}{x^2(t)+[y(t)+1]^2}dt, \tag{2.20}$$

where equations (2.11) and (2.13) have been used.

3. The linearized theory

If the dimensionless vortex strength ϵ is small, the solution $f(z)$ to equations (2.1)–(2.5) may be developed as a regular perturbation expansion in powers of ϵ, retaining only first-order terms. The resulting equations are then linear, and can be solved in closed form. This linearized solution is well known and is described fully by Kochin, Kibel' and Roze ([2], page 476) and Wehausen and Laitone ([1], page 489). For ease of reference, we shall summarize this solution here.

When ϵ is small, the complex potential is given by the expression

$$f(z) = z + \frac{i\epsilon}{2\pi}[\ln(z+i) - \ln(z-i)] + \frac{i\epsilon F^2}{\pi}\int_0^{\infty} \frac{e^{-ik(z-i)}dk}{1-kF^2} - \epsilon \exp\left(-\frac{i(z-i)}{F^2}\right) + O(\epsilon^2), \tag{3.1}$$

and the linearized formula for free-surface elevation is

$$\eta(x) = -\frac{\epsilon F^2}{\pi}\int_0^\infty \frac{e^{-k}\cos(kx)\,dk}{1-kF^2}$$

$$-\epsilon\, e^{-1/F^2}\sin\left(\frac{x}{F^2}\right) + O(\epsilon^2). \tag{3.2}$$

An alternative expression for the free-surface elevation is obtained by transforming the improper integral in equation (3.2) using contour integration as described, for example, by Havelock [10]. This results in the formula

$$\eta(x) = \frac{\epsilon F^2}{\pi}\int_0^\infty \frac{e^{-m|x|}[mF^2\cos m - \sin m]\,dm}{1+m^2F^4}$$

$$-2\epsilon H(x)\, e^{-1/F^2}\sin\left(\frac{x}{F^2}\right) + O(\epsilon^2), \tag{3.3}$$

where $H(x)$ is the Heaviside unit-step function having values 0 for $x < 0$ and 1 for $x > 0$. From equation (3.3) it is clear that

$$\eta(x) \to -A_1 \sin\left(\frac{x}{F^2}\right) + O(\epsilon^2) \qquad \text{as} \quad x \to \infty$$

where

$$A_1 = 2\epsilon\, e^{-1/F^2} \tag{3.4}$$

is the linearized wave amplitude.

For the wave resistance of the vortex, linearized theory gives

$$D = \epsilon^2 e^{-2/F^2} + O(\epsilon^3) = \tfrac{1}{4}A_1^2 + O(\epsilon^3), \tag{3.5}$$

as expected from conservation of energy. The linearized lift force acting on the vortex is

$$L = \epsilon F^2 - \frac{\epsilon^2 F^2}{4\pi} + \frac{\epsilon^2}{\pi} e^{-2/F^2}\mathrm{Ei}\left(\frac{2}{F^2}\right) + O(\epsilon^3), \tag{3.6}$$

where Ei denotes the exponential integral defined by Abramowitz and Stegun ([11], page 228).

4. Numerical methods

In this section we outline the numerical method used for the approximate solution of the non-linear equations (2.12)–(2.14) at N equally-spaced points $s_1, s_2, \ldots, s_N$ separated by an amount $h = s_j - s_{j-1}$, $j = 2, \ldots, N$. Points s_1 and s_N are supposed to correspond approximately to $-\infty$ and ∞ respectively. The numerical method used is a modification of that employed by Forbes and Schwartz [8].

The domain of integration of the integrodifferential equation (2.14) is first truncated upstream at s_1 and downstream at s_N, and the equation is then evaluated at the $N-1$ midpoints $s_{k-1/2}$, $k=2,\ldots,N$. Because the singularity in the integrand now occurs symmetrically between mesh points, the integral may be approximated by the trapezoidal rule, ignoring the singularity as described by Monacella [12].

Newton's method is used to solve for the vector of unknowns $[y_1', y_2', \ldots, y_N']^T$. However, the integrodifferential equation only provides $N-1$ equations since it was evaluated at the midpoints $x_{k-1/2}$, $k=2,\ldots,N$, and so an extra equation must be provided. This is, of course, the radiation condition (2.3).

The Newton's method algorithm for the solution of the nonlinear equations is therefore as follows:

Step 1: Satisfy the radiation condition (2.3) and Bernoulli's equation (2.12) by specifying

$$\begin{aligned} y_1 &= y_1' = 0, \\ x_1' &= \phi_1' = 1, \\ x_1 &= \phi_1 = s_1. \end{aligned} \tag{4.1}$$

Make an initial guess at the unknowns $y_2', \ldots, y_N'$; these are usually set to zero.

Step 2: Compute the remaining functions using equations (2.12) and (2.13) and trapezoidal-rule integration. Thus

$$\begin{aligned} x_k' &= \left(1 - y_k'^2\right)^{1/2}, \\ x_k &= x_{k-1} + \tfrac{1}{2}h(x_k' + x_{k-1}'), \\ y_k &= y_{k-1} + \tfrac{1}{2}h(y_k' + y_{k-1}'), \\ \phi_k' &= \left(1 - 2y_k/F^2\right)^{1/2}, \\ \phi_k &= \phi_{k-1} + \tfrac{1}{2}h(\phi_k' + \phi_{k-1}'), \quad k = 2,\ldots,N. \end{aligned} \tag{4.2}$$

Step 3: Obtain function values at half-grid points by interpolation:

$$\begin{aligned} x_{k-1/2} &= \tfrac{1}{2}(x_{k-1} + x_k), \\ y_{k-1/2} &= \tfrac{1}{2}(y_{k-1} + y_k), \\ x_{k-1/2}' &= \tfrac{1}{2}(x_{k-1}' + x_k'), \\ \phi_{k-1/2}' &= \tfrac{1}{2}(\phi_{k-1}' + \phi_k'), \quad k = 2,\ldots,N. \end{aligned} \tag{4.3}$$

Step 4: Compute the vector of residual errors in the satisfaction of the discretized

integrodifferential equation (2.14):

$$E_k = \frac{h}{\pi} \sum_{j=1}^{N} w_j \frac{(\phi_j' - x_j')(y_j - y_{k-1/2}) + y_j'(x_j - x_{k-1/2})}{(x_j - x_{k-1/2})^2 + (y_j - y_{k-1/2})^2}$$

$$+ \frac{\epsilon(y_{k-1/2} + 1)}{\pi\left[x_{k-1/2}^2 + (y_{k-1/2} + 1)^2\right]} + 1 - \phi_{k-1/2}' x_{k-1/2}',$$

$$k = 2, \ldots, N. \tag{4.4}$$

Here, w_j denotes the trapezoidal-rule weights, $w_1 = w_N = 1/2$ and $w_j = 1$, $j = 2, \ldots, N-1$.

Step 5: Compute a correction vector $[\Delta_2, \Delta_3, \ldots, \Delta_N]^T$ by solving the matrix equation

$$\sum_{j=2}^{N} \left[\frac{\partial E_k}{\partial y_j'}\right] \Delta_j = -E_k, \quad k = 2, \ldots, N. \tag{4.5}$$

The derivatives are computed numerically, by forward differencing. The vector $[\Delta_2, \Delta_3, \ldots, \Delta_N]^T$ is added to the vector $[y_2', y_3', \ldots, y_N']^T$ to create a new approximation to the derivatives $y_2', \ldots, y_N'$ and the programme is returned to step 2, unless the Euclidean norm $\|E\|$ of the vector of residual errors is sufficiently small, at which point the programme is stopped. If the new approximation *increases* $\|E\|$ rather than decreasing it, as required, then each element of the correction vector is halved, and the step repeated.

We have programmed the algorithm (4.1)–(4.5) in the FORTRAN language on an NAS 6630 computer. Five iterations are typically required to obtain convergence with $\|E\| < 10^{-8}$, and when $N = 141$, the programme takes about 11 minutes of execution time.

Once the values of the dependent variables are known at the surface, the formulae (2.19) and (2.20) for the drag and lift are evaluated by straightforward numerical quadrature.

5. Presentation of results

This chapter discusses the major differences between the predictions of the linearized theory summarized in Section 3 and the non-linear results obtained with the numerical method outlined in Section 4. It will suffice here to present results at the fixed Froude number $F = 0.7$, since the behaviour of the solution at other Froude numbers is qualitatively similar.

Figure 3 shows the drag as a function of absolute vortex strength $|\epsilon|$, for $F = 0.7$. The linearized result is computed from equation (3.5) and is shown as a solid line on the figure; note that linearized wave resistance is insensitive to the sign of ϵ. By contrast, the non-linear results are strongly dependent upon the direction of flow around the vortex as is evident from Figure 3, in which non-linear results for positive ϵ are indicated by triangles and results for negative circulation are indicated by circles.

The non-linear results for both positive and negative circulation agree well with

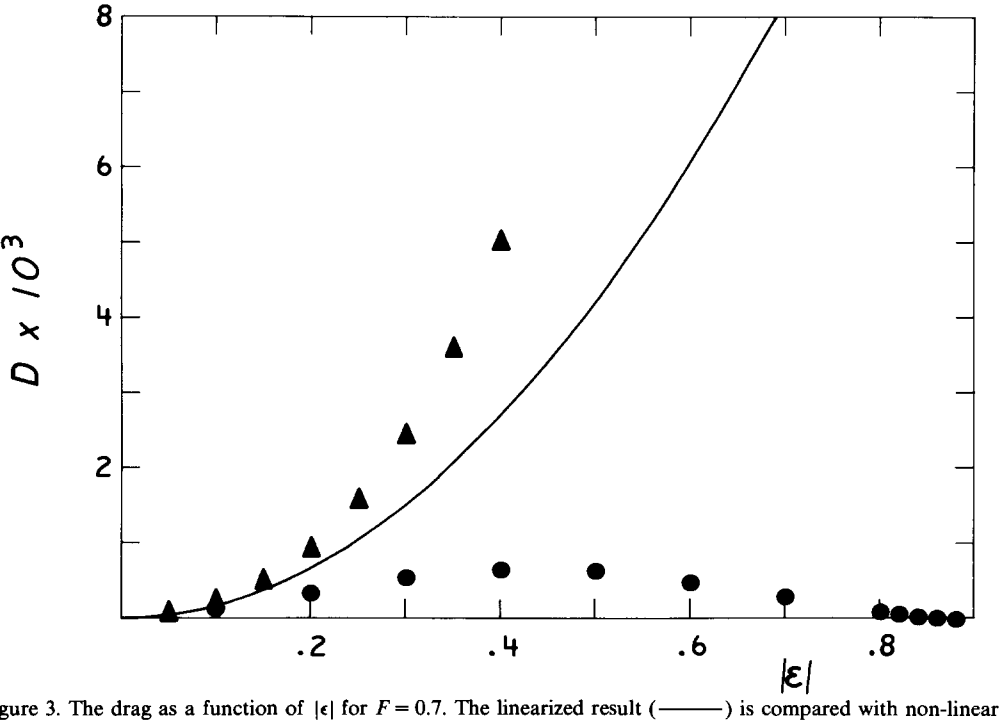

Figure 3. The drag as a function of $|\epsilon|$ for $F = 0.7$. The linearized result (———) is compared with non-linear results for positive and negative circulation, indicated by triangles and circles respectively.

linearized theory for small values of $|\epsilon|$, as is to be expected, although the two sets of results diverge strongly as $|\epsilon|$ is increased. For positive circulation, $\epsilon > 0$, the non-linear wave drag becomes significantly larger than that suggested by linearized theory, until, at $\epsilon = 0.4$ the non-linear result is some 85% larger than its linearized counterpart. Newton's method did not converge for $\epsilon = 0.41$, and we conclude that $\epsilon = 0.4$ is about the largest value of the vortex strength for which solutions of this type exist for $F = 0.7$.

The results for negative circulation in Figure 3 are perhaps a little surprising, since the non-linear drag is much smaller than the linearized drag, except for small $|\epsilon|$ when the two results are in agreement. The same trend was noted by Salvesen and von Kerczek [6] although we have apparently been able to obtain solutions for much larger values of $|\epsilon|$ than did those authors. Indeed, the results shown in Figure 3 are remarkable, since the non-linear wave resistance for negative circulation first increases with $|\epsilon|$, attaining a maximum at about $\epsilon = -0.4$, and then *decreases* as $|\epsilon|$ is increased, becoming extremely small at $\epsilon = -0.88$, which represents the largest value of $|\epsilon|$ for which Newton's method converged. Of course, the numerical method does not give a non-linear wave drag of *exactly* zero for $\epsilon = -0.88$, but we believe that this family of solutions is ultimately limited by a configuration having exactly zero wave resistance. This will be discussed shortly.

The lift is shown as a function of $|\epsilon|$ in Figure 4, for $F = 0.7$. In order that the differences between linearized and non-linear values may be highlighted, the first-order contribution ϵF^2 has been subtracted. The linearized result computed from equation (3.6) is indicated by a solid line, whilst non-linear values computed from equation (2.20) for positive and negative circulation are again indicated by triangles and circles, respectively.

In contrast to Figure 3, there is rather good agreement between the linearized theory and the non-linear results for positive circulation over the entire range $0 \leqslant \epsilon \leqslant 0.4$ in which solutions could be found, with values differing by a maximum of only about 9%. Agreement between linearized theory and non-linear values for negative circulation is also reasonable, except for very large values of $|\epsilon|$ when the non-linear values are significantly smaller than predicted by the linearized theory. The maximum difference occurs at $\epsilon = -0.88$, when the non-linear result is about 74% of the linearized value.

The behaviour of the linearized and non-linear wave resistance in Figure 3 may be understood by an examination of the corresponding free-surface profiles. In Figure 5 we show such a profile for the case $F = 0.7$, $\epsilon = 0.4$, which was the largest positive value of vortex strength for which Newton's method converged. The non-linear result is indicated with a solid line and the linearized elevation, computed from equations (3.2) and (3.3), by a dotted line. Far downstream the linearized elevation is given by the sine wave (3.4) whereas the non-linear surface elevation is expected to consist of a regular train of Stokes waves, the properties of which have been documented by Schwartz [13], for example. Note that the non-linear waves in Figure 5 possess the usual narrow crests and broader troughs. The peak-to-trough height of the non-linear waves is about 60% larger than that of the linearized sine waves, which explains to a large degree the difference between the linearized and non-linear wave drag for this case, presented in Figure 3.

Forbes and Schwartz [8] have discussed in detail the nature of the numerical errors to be expected from a method such as that used in this paper. For waves of moderate height, the errors are basically of two types. One source of error is the truncation of the domain of integration of the integrodifferential equation (2.14) upstream at the first point s_1. Since the conditions (4.1) imposed at this point do not exactly match the values of the dependent variables that would be obtained at s_1 from the true non-linear solution to the

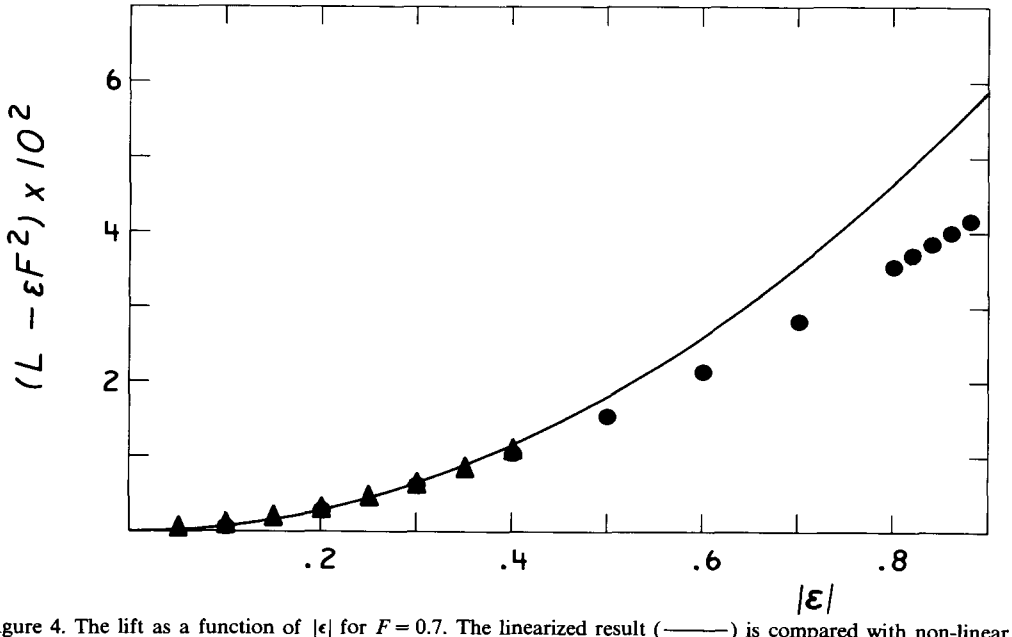

Figure 4. The lift as a function of $|\epsilon|$ for $F = 0.7$. The linearized result (———) is compared with non-linear results for positive and negative circulation, indicated by triangles and circles respectively.

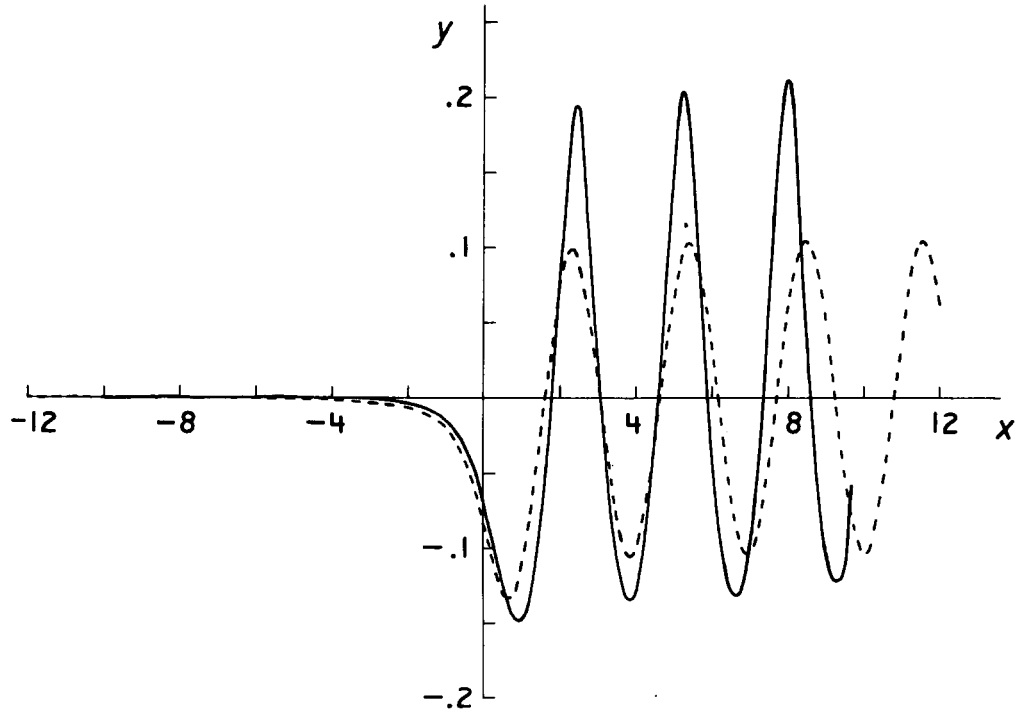

Figure 5. Linearized (— — —) and non-linear (———) wave profiles for $F = 0.7$, $\epsilon = 0.4$.

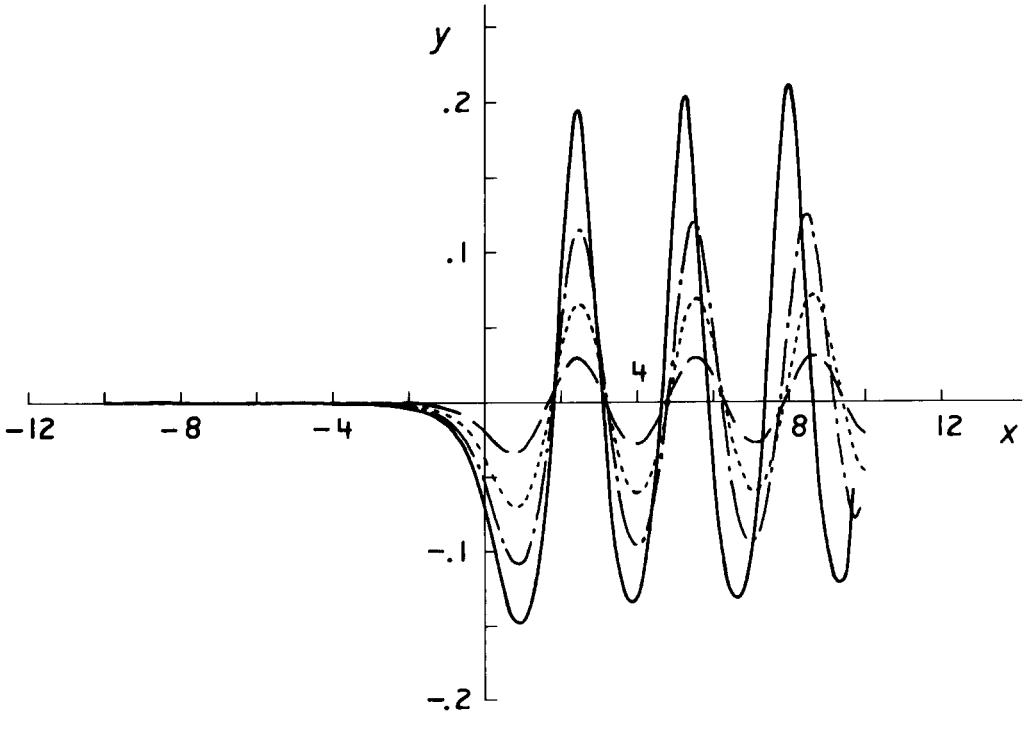

Figure 6. Free-surface elevations for four different vortex strengths, at $F = 0.7$. Profiles are shown for $\epsilon = 0.1$ (— — —), 0.2 (· · · · · ·), 0.3 (– · –) and 0.4 (———).

problem, the effect is that of an additional small disturbance imposed at s_1, and consequently, a spurious train of Stokes waves of very small amplitude appears upstream of the vortex. Such a train of numerically-produced waves is also present in the non-linear solution in Figure 5; it is, however, too small to be seen. The other source of error is the truncation of the domain of integration of equation (2.14) downstream at the last point s_N. This may be shown to affect only the last half-wavelength or so downstream. Of course, the usual roundoff and truncation errors are always present, but are only significant when the waves are very steep, since the curvature at the crests of such waves is too large to permit accurate computation in this region, given the relatively small number of free-surface grid points per wave cycle used here.

Following Salvesen and von Kerczek [6], we contrast the free-surface profiles at $F = 0.7$ obtained for several different values of the vortex strength. The results are shown in Figure 6, for $\epsilon = 0.1$, 0.2, 0.3 and 0.4. As the vortex strength ϵ is increased, the downstream waves increase uniformly in height, until, at about $\epsilon = 0.4$, a limiting configuration is presumably attained, in which the downstream waves possess sharp crests enclosing an angle of 120° and their steepness is approximately 0.141, as predicted by Schwartz [13]. Solutions of this type for larger values of ϵ would then not be possible.

The properties of the non-linear downstream waves in Figure 6 are presented in detail in Table 1. These data were computed from the numerical output by fitting a cubic spline $S(x)$ through the points (x_i, y_i), $i = 1, 2, \ldots, N$ to obtain the approximate free-surface elevation $\eta(x) \approx S(x)$. Let the values x_i^*, $i = 1, 2, 3$ denote respectively the positions of a trough, the next crest, and the next trough; they may be found approximately by solving

$$S'(x_i^*) = 0, \quad i = 1, 2, 3. \tag{5.1}$$

Equations (5.1) are solved by Newton's method. The wavelength is then

$$\lambda = x_3^* - x_1^*, \tag{5.2}$$

and the average free-surface elevation is

$$\bar{\eta} = \frac{1}{\lambda} \int_{x_1^*}^{x_3^*} S(x) \mathrm{d}x. \tag{5.3}$$

The cubic spline in equation (5.3) is integrated exactly. The wave steepness is approxi-

Table 1. Properties of the downstream waves at $F = 0.7$, as a function of vortex strength ϵ

ϵ	λ	Steepness	$\bar{\eta} \times 10^3$
0	3.07876	0	0
0.05	3.12	0.0087	0.19
0.1	3.11	0.0185	0.44
0.15	3.10	0.0295	0.78
0.2	3.08	0.0418	1.19
0.25	3.04	0.0558	1.68
0.3	2.99	0.0719	2.24
0.35	2.92	0.0915	2.83
0.4	2.79	0.120	3.56

mately

$$\text{steepness} = \frac{1}{\lambda}\left[S(x_2^*) - S(x_1^*)\right], \tag{5.4}$$

where λ is given by equation (5.2). The result in Table 1 for $\epsilon = 0$ is, of course, taken from the linearized solution (3.4), for which the wavelength is $\lambda = 2\pi F^2$.

From Table 1 it appears that the wavelength λ first increases slightly for small ϵ. Similar behaviour was noted by Salvesen and von Kerczek [6], but, as pointed out by those authors, this is probably evidence of a small numerical error which is more pronounced when the wave-slopes are small. Ultimately, however, the wavelength is a decreasing function of ϵ, as is evident from Figure 6.

The wave steepness, computed from equation (5.4), is also shown in Table 1 as a function of ϵ. Extrapolating the steepness to its theoretical maximum value of about 0.141 suggests that the maximum vortex strength for which solutions may be obtained is about 0.42, for $F = 0.7$. As mentioned previously, Newton's method did not converge beyond $\epsilon = 0.4$, presumably due to the high curvature at the wave crests.

Table 1 also shows the mean free-surface elevation as a function of ϵ. Because of the numerical error present in portions of the last wave downstream, described above, the average (5.3) was taken over the second of the downstream waves in Figure 6. We suspect that the mean free-surface elevation for this wave cycle is slightly below that of the Stokes waves which must be formed infinitely far downstream, and that the values of $\bar{\eta}$ in Table 1 are therefore a little low. However, the Table clearly indicates that $\bar{\eta}$ is a uniformly increasing function of ϵ. Note that the opposite trend is often the case in water of finite depth; for a discussion of this case the reader is referred to Benjamin [14], Salvesen and von Kerczek [6] and Forbes [15].

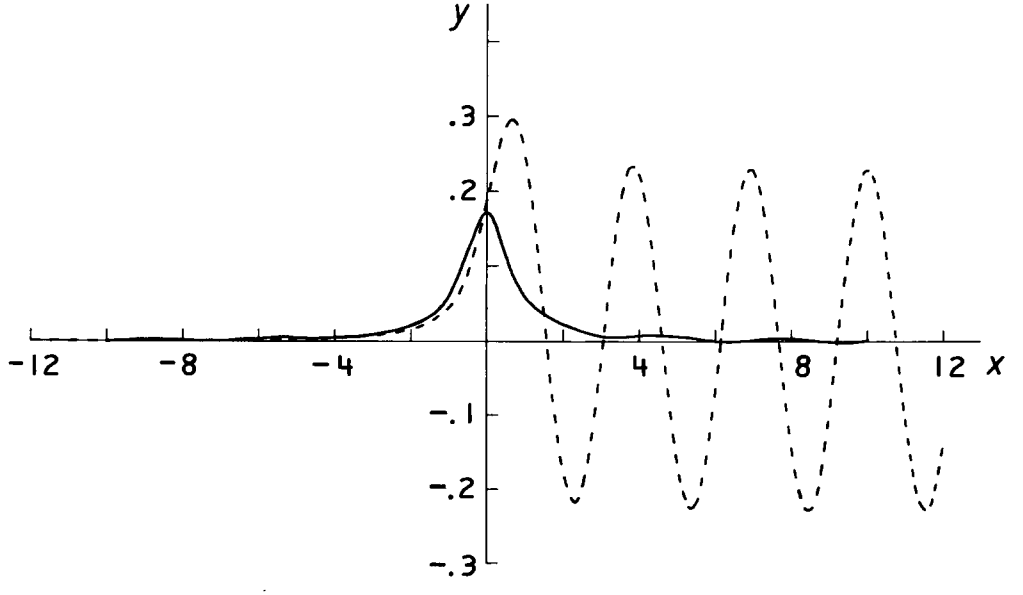

Figure 7. Linearized (— — —) and non-linear (———) wave profiles for $F = 0.7$, $\epsilon = -0.88$.

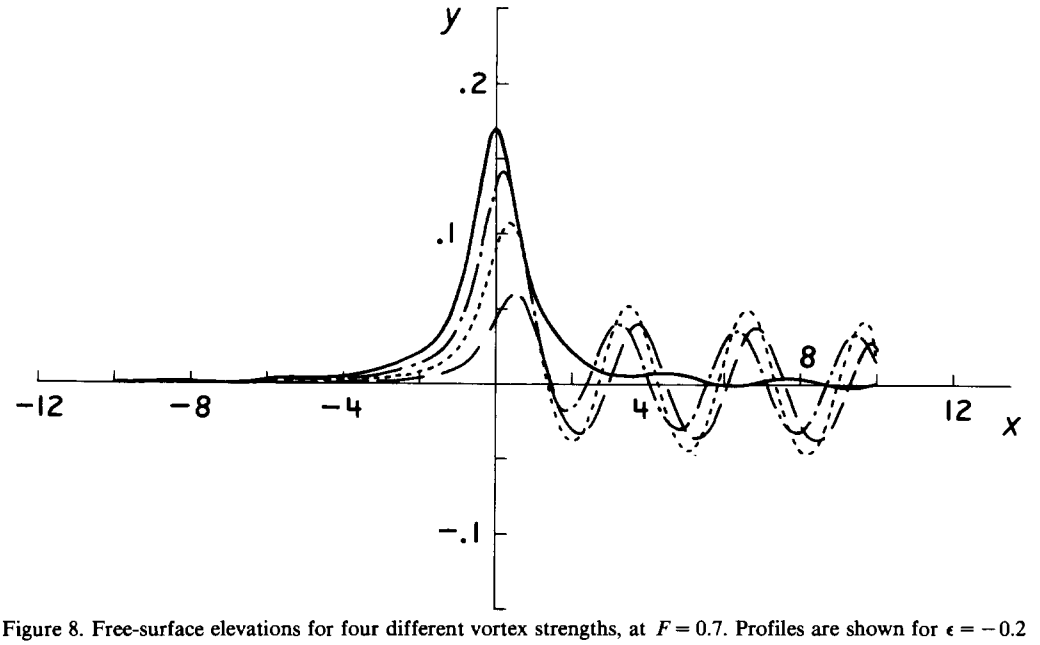

Figure 8. Free-surface elevations for four different vortex strengths, at $F = 0.7$. Profiles are shown for $\epsilon = -0.2$ (— — —), -0.4 (· · · · · ·), -0.6 (-·-) and -0.88 (———).

We turn now to perhaps the more interesting case of negative circulation. Figure 3 has already revealed that the wave resistance becomes essentially zero when $\epsilon = -0.88$ and $F = 0.7$, and the linearized and non-linear wave profiles for this case are shown in Figure 7. Here it is evident that the difference between the two wave profiles is extreme indeed. Linearized theory predicts a rise in the free surface slightly downstream of the vortex, followed by a train of sinusoidal waves of very large amplitude. By contrast, the non-linear free-surface profile is essentially symmetrical about the y-axis, possessing downstream waves of very small amplitude which accounts for the small non-linear drag.

By analogy with Figure 6, we present a progression of free-surface wave profiles in Figure 8, obtained with $F = 0.7$ and the four vortex strengths $\epsilon = -0.2$, -0.4, -0.6 and -0.88. As $|\epsilon|$ is increased, the downstream wave height first increases, reaching a maximum at about $\epsilon = -0.4$, and then decreases almost to zero at $\epsilon = -0.88$. The behaviour of the first wave crest is also of interest. For small $|\epsilon|$, it occurs a short distance downstream of the vortex, but as $|\epsilon|$ is increased, its position becomes closer to the y-axis, and, unlike the other downstream waves, its height increases uniformly with increasing $|\epsilon|$. As $|\epsilon|$ continues to increase, we conjecture that a limiting profile will be achieved, which is symmetric about the y-axis and has a sharp crest enclosing a 120° angle, and which possesses no waves and consequently has no wave drag. Solutions for larger values of $|\epsilon|$ would not be possible.

6. Summary and discussion

The non-linear problem of free-surface flow about a point vortex immersed in a running stream of infinite depth has been solved by an efficient numerical method which employs

only values of the dependent variables at the surface. Formulae have been derived for the drag and lift forces acting on the vortex, and are easily evaluated once the solution of the free-surface problem has been obtained.

Non-linear solutions have been obtained both for positive and for negative circulation at the vortex. When the circulation is positive, the free surface possesses a depression slightly downstream of the vortex, followed by a train of Stokes waves to infinity. The steepness and mean free-surface elevation of these waves are both increasing functions of the vortex strength, whilst the wavelength decreases as the vortex becomes stronger. For each value of the Froude number, there is some maximum vortex strength for which solutions exist, corresponding to the formation of sharp-crested waves downstream and the onset of wave breaking.

When the circulation about the vortex is negative, the free surface generally consists of an initial elevation downstream followed by a semi-infinite train of Stokes waves. As the vortex strength is increased, the amplitude of the downstream waves and the drag both increase initially, but then *decrease* again essentially to zero. For each Froude number, some maximum permissible vortex strength is believed to exist, at which the wave drag is precisely zero, and the free surface is wave-free, symmetrical upstream and downstream, and possesses a sharp crest enclosing an angle of 120° directly above the vortex. Work is currently in progress to attempt to obtain these drag-free solutions by the method of Forbes [16].

The apparent existence of drag-free non-linear solutions in the case of negative circulation may be of relevance to the design of underwater craft, since substantial drag reduction might be achieved by inducing negative circulation about the craft, perhaps by placing water-jets on its surface. In addition, such a vehicle would be difficult to detect visually, due to its absence of a downstream wave train. Of course, flow about real submarines is a three-dimensional phenomenon and is affected by viscosity through the formation of a boundary-layer and wake; nevertheless, an experimental investigation of such craft may prove profitable.

References

[1] J.V. Wehausen and E.V. Laitone, Surface waves. In: *Handbuch der Physik,* Vol. 9, Springer-Verlag (1960).

[2] N.E. Kochin, I.A. Kibel' and N.V. Roze, *Theoretical hydromechanics,* Wiley-Interscience (1964).

[3] R.W. Yeung, Numerical methods in free-surface flows, *Ann. Rev. Fluid Mech.* 14 (1982) 395–442.

[4] J.L. Hess, Progress in the calculation of nonlinear free-surface problems by surface-singularity techniques, *Proc. 2nd. Int. Conf. on Numerical Ship Hydrodynamics, Berkeley* (1977) 278–284.

[5] L.K. Forbes, Irregular frequencies and iterative methods in the solution of steady surface-wave problems in hydrodynamics, *J. Engineering Maths.* 18 (1984) 299–313.

[6] N. Salvesen and C. von Kerczek, Comparison of numerical and perturbation solutions of two-dimensional nonlinear water-wave problems, *J. Ship Research* 20 (1976) 160–170.

[7] M. Miksis, J.-M. Vanden Broeck and J.B. Keller, Axisymmetric bubble or drop in a uniform flow, *J. Fluid Mech.* 108 (1981) 89–100.

[8] L.K. Forbes and L.W. Schwartz, Free-surface flow over a semicircular obstruction, *J. Fluid Mech.* 114 (1982) 299–314.

[9] G.K. Batchelor, *An introduction to fluid dynamics,* Cambridge University Press (1967).

[10] T.H. Havelock, The method of images in some problems of surface waves, *Proc. Roy. Soc. London* A 115 (1927) 268–280.

[11] M. Abramowitz and I.A. Stegun (editors), *Handbook of mathematical functions,* Dover, Inc. New York (1972).

[12] V.J. Monacella, On ignoring the singularity in the numerical evaluation of Cauchy Principal Value integrals,

Hydromechanics laboratory research and development report no. 2356, David Taylor Model Basin, Washington D.C. (1967).

[13] L.W. Schwartz, Computer extension and analytic continuation of Stokes' expansion for gravity waves, *J. Fluid Mech.* 62 (1974) 553–578.

[14] T.B. Benjamin, Upstream influence, *J. Fluid Mech.* 40 (1970) 49–79.

[15] L.K. Forbes, Non-linear free-surface flows about blunt bodies, *Ph.D. thesis, University of Adelaide* (1981).

[16] L.K. Forbes, Non-linear, drag-free flow over a submerged semi-elliptical body, *J. Engineering Maths.* 16 (1982) 171–180.